

000 001 002 003 004 005 006 007 008 009 010 011 012 013 014 015 016 017 018 019 020 021 022 023 024 025 026 027 028 029 030 031 032 033 034 035 036 037 038 039 040 041 042 043 044 045 046 047 048 049 050 051 052 053 CONFORMALIZED PREDICTIONS IN HYPERGRAPH NEU- RAL NETWORKS VIA CONTRASTIVE LEARNING

Anonymous authors

Paper under double-blind review

ABSTRACT

Hypergraph representation learning has gained immense popularity over the last few years due to its applications in real-world domains like social network analysis, recommendation systems, biological network modeling, and knowledge graphs. However, hypergraph neural networks (HGNNs) lack rigorous uncertainty estimates, which limits their deployment in critical applications where the reliability of predictions is crucial. To bridge this gap, we propose Contrastive Conformal HGNN (CCF-HGNN) that jointly accounts for aleatoric and epistemic uncertainties in hypergraph-based models for guaranteed and robust uncertainty estimates. CCF-HGNN accounts for epistemic uncertainty in HGNN predictions by producing a prediction set that leverages the topological structure and provably contains the true label with a pre-defined coverage probability. It also accounts for aleatoric uncertainty by leveraging contrastive learning on the structure of the hypergraph. To enhance the power of the predictions, CCF-HGNN performs an additional auxiliary task of hyperedge degree prediction with an end-to-end differentiable sampling-based approach. Extensive experiments on real-world hypergraph datasets demonstrate the superiority of CCF-HGNN by improving the efficiency of prediction sets while maintaining valid coverage.

1 INTRODUCTION

Network-structured data underpins a broad spectrum of scientific and real-world applications, ranging from social interactions Newman (2003) and recommender systems Ying et al. (2018) to biological networks Zhang et al. (2022) and knowledge graphs Nickel et al. (2015). This has fueled the rapid growth of graph-based machine learning, where graph neural networks (GNNs) have emerged as a dominant paradigm for learning from relational data Kipf & Welling (2016); Hamilton et al. (2017); Velickovic et al. (2017). More recently, attention has shifted towards *hypergraph representation learning*, which extends beyond pairwise relations to model higher-order interactions, thereby offering a more faithful abstraction for many complex systems Battaglia et al. (2018); Zhang et al. (2018b). The expressive power of hypergraphs has led to applications across diverse domains, including healthcare (e.g., multiple patients sharing a room) Xu et al. (2022); Choudhuri et al. (2025a); Xu et al. (2023), social networks (e.g., users joining groups or channels) Li et al. (2013), bioinformatics Tian et al. (2009), and cyber-security Lin et al. (2024). To exploit these structures, hypergraph neural networks (HGNNs) have been developed with specialized message-passing and aggregation mechanisms Feng et al. (2019); Yadati et al. (2019); Bai et al. (2021), demonstrating superior performance when group-wise relations, rather than dyadic links, are essential.

The evolution of HGNNs has closely paralleled that of GNNs. Early work, such as HGNN Feng et al. (2019), adapted the message-passing framework of GCN Kipf & Welling (2016), while HCHA Bai et al. (2021) extended the attention mechanism of GAT Velickovic et al. (2017) to hypergraphs. More recent efforts have introduced advanced ideas, including multiset functions Chien et al. (2021), network diffusion Wang et al. (2023a), energy-based formulations Wang et al. (2023b), and implicit modeling Li et al. (2025); Choudhuri et al. (2025b). Despite these innovations, a key limitation persists: *existing HGNNs provide no mechanism to quantify predictive uncertainty*. This omission is particularly problematic in high-stakes domains, where decisions require not only accuracy but also calibrated confidence. A principled solution is to construct *prediction sets* that guarantee high-probability coverage for each sample. While numerous uncertainty quantification methods have been proposed in the broader machine learning literature Guo et al. (2017); Zhang et al. (2020); Hsu et al.

(2022); Zhang et al. (2018a); Gal & Ghahramani (2016); Trivedi et al. (2023); Lakshminarayanan et al. (2017), they generally lack rigorous coverage guarantees—i.e., assurances that the true label lies within the predicted set with the desired probability.

The field of conformal prediction, pioneered by Vovk et al. (2005), provides a principled framework for constructing prediction sets with rigorous, finite-sample coverage guarantees under minimal distributional assumptions. By calibrating nonconformity scores on held-out data, conformal prediction methods ensure that the true label is included in the prediction set with a user-specified probability (e.g., $1 - \alpha$), regardless of the underlying data distribution. This property has fueled widespread adoption in areas such as computer vision Angelopoulos & Bates (2021), natural language processing Kumar et al. (2023), and time-series forecasting Stankeviciute et al. (2021); Zaffran et al. (2022); Gibbs & Candes (2021). Conformal prediction has gained immense popularity in graph representation learning, with frameworks aimed at quantifying uncertainty in inductive Clarkson (2023); Zargarbashi & Bojchevski (2023) and transductive Zargarbashi et al. (2023); Huang et al. (2024) node classification and edge/link prediction Luo & Colombo (2024); Zhao et al. (2024); Choudhuri et al. (2025c).

While conformal prediction provides coverage guarantees, it explicitly quantifies epistemic uncertainty (i.e., model-specific uncertainty) while ignoring aleatoric uncertainty (i.e., data uncertainty). Moreover, as highlighted in Table 1, uncertainty quantification in hypergraph representation learning has not been studied before. Quantifying both sources of uncertainty is particularly important in hypergraphs, as data often appears in the form of higher-order relationships (e.g., co-authorship, biochemical complexes, and co-purchases) that are prone to noise, sparsity, and lack of standardization, limiting effective model training in practice. Unlike graphs, where uncertainty typically stems from missing or spurious edges, hypergraphs are subject to structural ambiguity in the semantics of multi-way relations (e.g., “all authors of a paper” or “all participants in a discussion”), which introduces additional sources of noise. Furthermore, in node classification tasks, a single mislabeled node does not merely affect its immediate neighbors, as in graphs, but can propagate errors to every node within the same hyperedge, significantly amplifying the impact of label noise.

To address these challenges, we introduce *Contrastive Conformal Hypergraph Neural Network (CCF-HGNN)*, an end-to-end framework that jointly models aleatoric and epistemic uncertainty in hypergraph representation learning. Our contributions are as follows:

- To the best of our knowledge, this is the first work that combines aleatoric uncertainty (contrastive augmentation- aided learning) and epistemic uncertainty (conformal prediction).
- We propose an auxiliary hyperedge-degree prediction task to our overall conformal training algorithm to boost the power of the hypergraph representations. We additionally propose an efficient computational method to sample the important hyperedges based on the augmentation strategy and perform the hyperedge-degree prediction task only on those hyperedges.
- We provide theoretical evidence that guarantees that the joint modeling of epistemic and aleatoric uncertainties is both efficient (ie, the predictive bands returned are shorter) and effective (empirical coverage provably exceeds the given confidence level).
- Extensive experiments on several real-world hypergraph datasets for uncertainty quantification in the node classification task demonstrate the overall utility of our method.

2 PRELIMINARIES

Let $H = (\mathcal{V}, \mathcal{E}, \mathcal{X}, \mathcal{Y})$ be a hypergraph, where \mathcal{V} is a set of nodes, \mathcal{E} is a set of hyperedges, and $\mathcal{X} = \{\mathbf{x}_v\}_{v \in \mathcal{V}}$ is the set of node attributes, where $\mathbf{x}_v \in \mathbb{R}^d$ is a d -dimensional feature vector for node $v \in \mathcal{V}$. Let $\mathcal{Y} = \{y_v\}_{(v) \in \mathcal{V}}$ be the set of node labels. Our paper focuses on classification problems,

Table 1: Comparison of the features of the prior works. Our proposed framework jointly accounts for epistemic and aleatoric uncertainties while maintaining valid marginal coverage.

| Method | Coverage | Epistemic | Aleatoric |
|-----------------------------|----------|-----------|-----------|
| TS and VS Guo et al. (2017) | ✗ | ✗ | ✓ |
| ETS Zhang et al. (2020) | ✗ | ✗ | ✓ |
| CF-GNN Huang et al. (2024) | ✓ | ✓ | ✗ |
| Ours | ✓ | ✓ | ✓ |

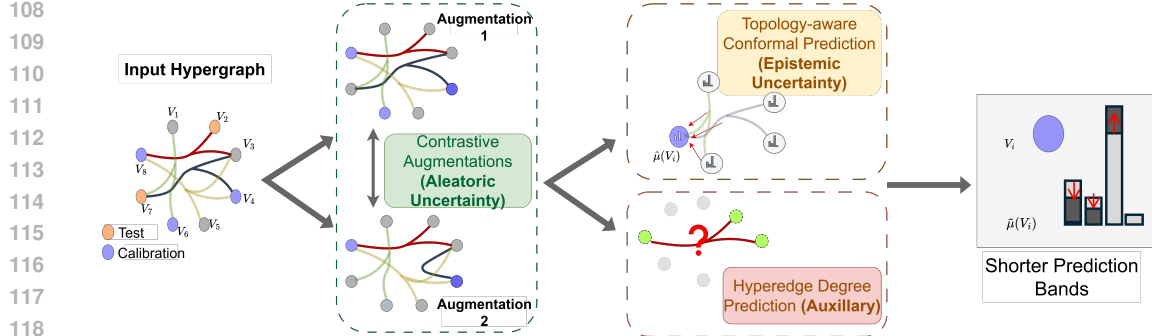


Figure 1: **Contrastive Conformal Hypergraph Neural Network:** The overall framework minimizes three losses: 1) Contrastive Loss: Structural alterations generate multiple views of the hypergraph, encouraging the model to learn invariant representations. 2) Conformal Inefficiency Loss: Topology-aware conformal loss ensures similarity in uncertainties of a node based on its local neighbors (nodes that share hyperedges). 3) Degree Loss: Predicting the hyperedge degree of a sample of hyperedges to guide the model to learn the structure. This leads to shorter and more confident prediction bands.

but our theory and method naturally extend to regression problems. To perform point predictions, we are given a mean estimator $\hat{\mu}$ that predicts the node label \hat{y}_v given the node embedding x_v .

2.1 TRANSDUCTIVE SETTING

We focus on the transductive node classification problem with a random data split akin to Huang et al. (2024). In this setting, we partition the node labels into three disjoint sets: $\mathcal{Y}_{\text{train}}$, \mathcal{Y}_{cal} , and $\mathcal{Y}_{\text{test}}$. This leads to *training* data $D_{\text{train}} = (\mathcal{V}, \mathcal{E}, \mathcal{X}, \mathcal{Y}_{\text{train}})$, *calibration* data $D_{\text{cal}} = (\mathcal{V}, \mathcal{E}, \mathcal{X}, \mathcal{Y}_{\text{cal}})$, and *testing* data $D_{\text{test}} = (\mathcal{V}, \mathcal{E}, \mathcal{X}, \mathcal{Y}_{\text{test}})$. In particular, during training, the model can access $\mathcal{V}, \mathcal{E}, \mathcal{X}$, but only the training labels $\mathcal{Y}_{\text{train}}$ are revealed to the model. Abusing the notation, we use $\mathcal{V}_{\text{train}}$ to denote elements of \mathcal{V} for which the node labels are in $\mathcal{Y}_{\text{train}}$. We follow the same notation throughout the paper. After training, the calibration data $\{y_v\}_{v \in \mathcal{V}_{\text{cal}}}$ is used to construct uncertainty estimates. Finally, we predict the uncertainty bands for the remaining nodes (i.e., $\mathcal{V}_{\text{test}}$).

2.2 MEAN ESTIMATOR: HYPERGRAPH NEURAL NETWORK

Hypergraph Neural Networks (HGNNS) are powerful machine learning models that leverage the high-order network structure during message passing. Unlike traditional graph neural networks that only aggregate pairwise information, HGNNS can handle the complexity of hypergraphs, where relationships between nodes are generalized beyond pairwise connections. Like Graph Neural Networks (GNNs), HGNNS aggregate neighborhood information Bai et al. (2021); Feng et al. (2019) via a sequence of propagation layers where each layer consists of a Message Passing Step, and a Node Update Step. Further details about the propagation steps are provided in the Appendix A.1.

2.3 CONFORMAL PREDICTION

In this work, we focus on split conformal prediction Vovk et al. (2005), which proceeds in four primary steps. Given a miscoverage rate $\alpha \in [0, 1]$, the steps are: **(1) Training:** Train the mean estimator $\hat{\mu}$ on the training data D_{train} . **(2) Calibration:** For each node v in \mathcal{V}_{cal} , compute the non-conformity scores (heuristic notion of how off the prediction is from the true label) $\{V(\mathbf{x}_v, y_v)\}_{v \in \mathcal{V}_{\text{cal}}}$ and create an empirical distribution from the scores. **(3) Quantile Computation:** Compute the $(1 - \alpha)^{\text{th}}$ quantile $\hat{Q}_{1-\alpha}$ of the distribution $\frac{1}{|\mathcal{V}_{\text{cal}}|+1} \sum_{v \in \mathcal{V}_{\text{cal}}} \delta_{V_v} + \delta_\infty$, where δ_a is Dirac Delta distribution at point a , and V_v is shorthand for $V(\mathbf{x}_v, y_v)$. **(4) Band Computation:** Given a test node v and corresponding feature \mathbf{x}_v , a prediction set/interval $\hat{C}(\mathbf{x}_v) = \{y \in \mathcal{Y} : V(\mathbf{x}_v, y) \leq \hat{Q}_{1-\alpha}\}$ is constructed. The notion of transferring the prediction bands computed on the calibration data to the points in test data relies on the following permutation invariance assumption Huang et al. (2024); Zargarbashi & Bojchevski (2023).

162 **Assumption 1.** For any permutation π on the calibration and test nodes, the non-conformity score V
 163 obeys

$$165 \quad V(\mathbf{x}_v, y_v; \{y_a\}_{(a) \in \mathcal{V}_{train \cup cal}}, \mathcal{X}, \mathcal{V}, \mathcal{E}) = V(\mathbf{x}_v, y_v; \{y_a\}_{(a) \in \mathcal{V}_{train \cup cal}}, \mathcal{X}, \mathcal{V}_\pi, \mathcal{E})$$

166 This means that the non-conformity scores of nodes in a hypergraph H are exchangeable.

168 Assumption 1 imposes the permutation invariance condition for the HGNN training to later compute
 169 the non-conformity scores for node prediction, which means that the model output/non-conformity
 170 score is invariant to permuting the order of the calibration and test nodes on the hypergraph. HGNNs
 171 do not rely on the ordering of the nodes, hence they typically satisfy the assumption.

172 **Lemma 1.** (Coverage Guarantee for Conformal Inference) Vovk et al. (2005); Tibshirani et al.
 173 (2019) Under Assumption 1, for any $\alpha > 0$, the confidence band returned by the conformal inference
 174 algorithm satisfies:

$$175 \quad \mathbb{P}(y_v \in \hat{C}_{1-\alpha}(\mathbf{x}_v)) \geq 1 - \alpha \quad (1)$$

176 where the probability is taken over the calibration fold D_{cal} and the testing point (\mathbf{x}_v, y_v) .

177 Here, $\mathbb{P}(y_v \in \hat{C}_{1-\alpha}(\mathbf{x}_v))$ denotes the **coverage**, i.e., the probability that the true label y_v lies in the
 178 predictive band.
 179

180 3 OUR METHOD

183 In this section, we propose our method, Contrastive Conformal Hypergraph Neural Network (CCF-
 184 HGNN), which aims to reduce the size of the predictive band length while maintaining coverage for
 185 hypergraph neural networks. The main idea is to boost the APS and RAPS scores (see section 4.1)
 186 with the help of local topological information and account for data-noise in the form of contrastive
 187 augmentations.

188 3.1 COMPUTING DIFFERENTIABLE INEFFICIENCY LOSS

190 Instead of using pairwise local topological information as done by Huang et al. (2024), our work
 191 uses high-order local topological information that goes beyond homophily or other aggregation
 192 mechanisms (like mean, sum, etc.). To implement this idea, we use a separate HGNN learner $\hat{\mu}$
 193 parameterized by the weights ϑ for the same hypergraph network H with node features initialized by
 194 $\hat{\mu}(\mathcal{X})$. Here $\hat{\mu}(\cdot)$ denotes the mean estimator that has been used during the training process. Given
 195 $\hat{\mu}(\mathcal{X}) = \text{HGNN}_\vartheta(\hat{\mu}(\mathcal{X}), H)$, and a target miscoverage rate α , we partition the calibration data D_{cal}
 196 into $D_{corr-cal}$ (correction subset) and $D_{cal-test}$ (testing subset) compute a differentiable loss in the fol-
 197 lowing steps: 1) **Differentiable Quantile Computation:** Compute the smooth differentiable quantile
 198 $\hat{\eta} = \text{DiffQuantile}(\{V(\mathbf{x}_i, y_i) \mid i \in \mathcal{D}_{corr-cal}\})$ on $D_{corr-cal}$. 2) **Inefficiency Proxies Computation:**
 199 Construct a differentiable proxy of the miscoverage on $D_{cal-test}$ by using $D_{corr-cal}$ as calibration data.
 200 For class k and node i in $D_{cal-test}$, the non-conformity score is given as $V(\mathbf{x}_i, k)$ (as per APS and
 201 RAPS scores). The inefficiency proxy will thus be $c_i = \sigma\left(\frac{V(\mathbf{x}_i, k) - \hat{\eta}}{\tau_1}\right)$, where $\sigma(\cdot)$ denotes the
 202 sigmoid function and τ_1 denotes the temperature hyperparameter Stutz et al. (2022). 3) **Overall**
 203 **Loss Computation:** Compute the overall inefficiency loss as an average of the inefficiency proxies
 204 $\mathcal{L}_{\text{Ineff}} = \frac{1}{m} \sum_{i \in \mathcal{D}_{cal-test}} \frac{1}{|\mathcal{Y}|} \sum_{k \in \mathcal{Y}} c_i$.

205 The proof that the inefficiency loss is exchangeable simply follows the proof of the same theorem
 206 given in Huang et al. (2024) as our setup also operates on the transductive setting, and hypergraphs
 207 can be represented as graphs through clique/star expansions Agarwal et al. (2006). Note that while
 208 the number of edges changes due to these expansions, the number of nodes remains the same, which
 209 is why the proof holds.

211 3.2 USING CONTRASTIVE AUGMENTATIONS

213 While inefficiency quantifies a measure of the epistemic uncertainty, we have not yet accounted for
 214 the aleatoric uncertainty that can arise from a multitude of data-dependent properties. Minimizing
 215 the proxy of the epistemic uncertainty in isolation exposes our framework to noise that can arise
 from the structure of the hypergraph. As HGNNs rely on aggregating information by exploiting

216 the structural properties of hypergraphs, aleatoric uncertainties will be amplified by the model if
 217 unaccounted for. This motivated us to quantify and minimize the aleatoric uncertainty jointly with
 218 the epistemic uncertainty.

219 To execute this motivation, we utilize contrastive augmentations to boost the power of node em-
 220 beddings in a self-supervised manner. We design contrastive structural augmentations akin to a
 221 prior work Wei et al. (2022) by constructing augmentations $\mathcal{H}_1 = \hat{f}(H, A_1)$ $\mathcal{H}_2 = \hat{f}(H, A_2)$ and
 222 corresponding node embeddings where $\hat{f}(\cdot, \cdot)$ is a function that perturbs the structure of a hypergraph
 223 given a perturbation schema A . Hence, A_1 and A_2 are two instantiations of the perturbation schema.
 224 Finally, we can obtain the node embeddings of the augmented hypergraphs as $\mathbf{Z}^1 = \tilde{\mu}(\mathcal{H}_1, \mathbf{X})$
 225 $\mathbf{Z}^2 = \tilde{\mu}(\mathcal{H}_2, \mathbf{X})$ and minimizing the contrastive loss as follows:

$$227 \quad \mathcal{L}_{\text{Contra}} = \text{InfoNCE}(\mathbf{Z}^1, \mathbf{Z}^2, \tau_2) = -\sum_{i=1}^{|\mathcal{V}|} \log \frac{\exp\left(\frac{\text{sim}(\mathbf{z}_i^1, \mathbf{z}_i^2)}{\tau_2}\right)}{\sum_{j=1}^{|\mathcal{V}|} \exp\left(\frac{\text{sim}(\mathbf{z}_i^1, \mathbf{z}_j^2)}{\tau_2}\right)}, \quad (2)$$

231 Here τ_2 is a temperature hyperparameter to the popular InfoNCE loss Chen et al. (2020) and $\text{sim}(\cdot)$
 232 denotes a similarity function like cosine similarity. The contrastive loss is also exchangeable as the
 233 loss depends on the embeddings, which are thus dependent on the mean estimator (HGNN in this
 234 case). As HGNN is permutation invariant, the contrastive loss is also exchangeable.

235 3.3 BOOSTING CONTRASTIVE AUGMENTATION WITH AUXILIARY HYPEREDGE DEGREE 236 PREDICTION

238 To appropriately guide the calibration model $\tilde{\mu}(\cdot)$ with the structure of the hypergraph, we propose
 239 jointly training the hypergraph augmentations with the task of predicting the original hyperedge
 240 degrees. However, as the number of hyperedges in real-world hypergraphs is much greater than
 241 the number of nodes, we propose an efficient augmentation strategy to sample the most important
 242 hyperedges to perform the auxiliary hyperedge degree prediction task.

243 Let the hyperedge-Laplacian matrix of the hypergraph be $\mathbf{L} \in \mathbb{R}^{m \times n}$, where $m = |\mathcal{E}|$ is the number
 244 of hyperedges and $n = |\mathcal{V}|$ is the number of nodes. The hyperedge-Laplacian can be computed
 245 as $\mathbf{L} = \mathbf{D}_e^{-\frac{1}{2}} \mathbf{H}^T \mathbf{D}_v^{-\frac{1}{2}}$ Feng et al. (2019), where \mathbf{H} denotes the incidence matrix. We apply self-
 246 attention mechanism Vaswani et al. (2017) over the hyperedge Laplacian to get attention weights
 247 $a_j = \text{Self-Attention}(\mathbf{L}_{:,j})$ for each hyperedge index j .

248 To sample the k most important hyperedges in a fully differentiable manner, we use the Gumbel-
 249 Softmax trick Jang et al. (2016) as $\mathbf{s} = \text{GumbelSoftmax}(\mathbf{a}, k, \tau_3)$, where $\mathbf{s} \in \mathbb{R}^n$ is a soft selection
 250 mask, k is the desired number of hyperedges, and τ_3 is the temperature parameter. The auxiliary
 251 hyperedge degree prediction task is then $\hat{d}_j = h(\mathbf{L}_{:,j})$, where $h(\cdot)$ is a learnable predictor and \hat{d}_j is
 252 the predicted degree of hyperedge e_j . Given the true degree d_j for the hyperedge in the augmented
 253 hypergraph, the loss for the degree prediction task is $\mathcal{L}_{\text{deg}} = \sum_{j=1}^n s_j \cdot \ell(\hat{d}_j, d_j)$ where $\ell(\cdot, \cdot)$ is a
 254 regression loss, e.g., mean squared error. The degree prediction loss is also exchangeable as it does
 255 not relate to node labels in the transductive setting.

257 The overall training algorithm of our method is given in Algorithm 1 in the Appendix. This joint
 258 training encourages the model to learn representations sensitive to the structure of the most informative
 259 hyperedges while maintaining differentiability for end-to-end optimization.

261 3.4 THEORETICAL GUARANTEE

263 This section provides theoretical guarantees for our proposed method, in terms of shorter uncertainty
 264 band length (compared to the naive extension of the graph counterpart Huang et al. (2024) to
 265 hypergraphs). We will first define some notations that form the foundation of our theoretical results.

266 **Notations:** Assume an encoder-decoder architecture of the conformal corrector $\tilde{\mu}(\cdot)$, where the
 267 encoder maps the input node features to latent embeddings and the decoder maps those embeddings to
 268 predictions. Consider two models: (1) **CF-HGNN:** $\mathbf{Z}_0 = h_0(\mathcal{X})$ and $\hat{Y} = g_0(\mathbf{Z}_0)$ where $h_0(\cdot)$ and
 269 $g_0(\cdot)$ is the encoder and decoder, and \mathbf{Z}_0 is the latent representation. Its prediction set has expected

size $\mathcal{C}_0(\mathbf{x})$ given the node embedding \mathbf{x} . This is the naive extension of Huang et al. (2024) to hypergraphs. (2) **CCF-HGNN**: $\mathbf{Z}_1 = h_1(\mathcal{X}, A)$ and $\hat{\mathbf{Y}}_1 = g_1(\mathbf{Z}_1)$ where $h_1(\cdot)$ and $g_1(\cdot)$ is encoder and decoder, and \mathbf{Z}_1 is the latent representation under contrastive augmentation A . Its prediction set has expected size $\mathcal{C}_1(\mathbf{x})$ given the node embedding \mathbf{x} . Recall, this is our proposed approach.

Lemma 2. *Let $I(Y; \mathbf{Z}_1)$ and $I(Y; \mathbf{Z}_0)$ denote the mutual information between the labels and latent embeddings for CCF-HGNN and CF-HGNN, respectively, and $\Delta \in \mathbf{R}^+$ then,*

$$I(Y; \mathbf{Z}_1) \geq I(Y; \mathbf{Z}_0) + \Delta. \quad (3)$$

The proof is provided in Appendix A.2. Using the results from Lemma 2, we can prove the following theorem on the expected band length produced by CCF-HGNN and CF-HGNN.

Theorem 1. *Under the assumptions:*

1. **Bounded coverage:** *Contrastive augmentations do not reduce conformal coverage (marginal coverage $\geq 1 - \alpha$ is preserved on average).*
2. **Large Mutual Information gap:** $I(Y; \mathbf{Z}_1) - I(Y; \mathbf{Z}_0)$ is sufficiently large (Lemma 2).

Then, the expected conformal prediction set size under CCF-HGNN is smaller than under CF-HGNN:

$$\mathbb{E}[|\mathcal{C}_1(\mathbf{x})|] \leq \mathbb{E}[|\mathcal{C}_0(\mathbf{x})|]. \quad (4)$$

The proof is provided in Appendix A.3. We also have a theoretical result on the band-length convergence guarantee for CCF-HGNN in the Appendix A.4..

4 EXPERIMENTS

Following the theoretical guarantees discussed earlier, we next demonstrate the empirical superiority of our proposed framework. Specifically, we evaluate the performance of our model and compare its performance against several non-trivial baselines on real-world datasets. We will first provide details about the experimental setup and then proceed to describe the evaluation metrics and experimental protocols, followed by the results.

4.1 SETUP

We conducted all experiments on AMD EPYC 7763 64-Core Processor with 1.08 TB memory and 8 NVIDIA A40 GPUs with CUDA version 13.0. Our code and experimental setup, including data construction, are available for peer review¹.

Datasets: We evaluated the performance of our proposed framework on four real-world datasets used in prior works Chien et al. (2021); Wang et al. (2023a). The datasets include co-authorship datasets like DBLP Yadati et al. (2019), co-purchases large dataset like Walmart-Trips Amburg et al. (2020), and co-voting datasets like House-Bills Chodrow et al. (2021), and Congress Fowler (2006). Summary statistics and further descriptions are provided in the Appendix A.5.

Baseline Methods: As there are no prior works tailored to quantify uncertainty for hypergraphs specifically, we use traditional uncertainty quantification methods (that do not provide statistical coverage guarantees) as baseline methods. These include Temperature Scaling (TS) Guo et al. (2017), Vector Scaling (VS) Guo et al. (2017), and Ensemble Temperature Scaling (ETS) Zhang et al. (2020). Additionally, we adapt traditional conformal prediction methods by adopting an HGNN mean estimator to obtain point predictions on hypergraphs (CP). Finally, we adapted the SOTA conformal prediction method for GNNs Huang et al. (2024) to aggregate information and perform conformal prediction in hypergraphs (CF-HGNN). Detailed descriptions of the baselines are provided in the Appendix A.6.

Non-Conformity Score Functions: We evaluate two popular conformal prediction scores.

¹https://anonymous.4open.science/r/cont_conf_ml-3EB9

(1) **APS (Adaptive Prediction Sets)** **Romano et al. (2020)**: For a model outputting class probabilities $\hat{p}(y | \mathbf{x})$, let $\pi(\mathbf{x})$ denote the ordering of labels sorted by decreasing probability. The APS score for class y is defined as $V_{\text{APS}}(\mathbf{x}, y) = \sum_{j: \pi_j(\mathbf{x}) \prec y} \hat{p}(\pi_j(\mathbf{x}) | \mathbf{x}) + U \cdot \hat{p}(y | \mathbf{x})$, where $U \sim \text{Unif}(0, 1)$ and $\pi_j(\mathbf{x}) \prec y$ means label $\pi_j(\mathbf{x})$ is ranked higher than y . APS adaptively constructs prediction sets by accumulating probabilities until the threshold calibrated by conformal prediction is reached.

(2) **RAPS (Regularized Adaptive Prediction Sets)** **Angelopoulos et al. (2020)**: RAPS extends APS by adding a regularization term that penalizes large set sizes. For class y , the score is $V_{\text{RAPS}}(\mathbf{x}, y) = S_{\text{APS}}(\mathbf{x}, y) + \lambda \cdot |\{j : \pi_j(\mathbf{x}) \prec y\}|^\gamma$, where $\lambda \geq 0$ controls the strength of the penalty and $\gamma \geq 1$ controls its growth rate. This modification encourages tighter prediction sets while preserving coverage guarantees.

Evaluation Metrics: We randomly split data into train, validation, calibration-test folds with a 20:30:50 split ratio. We adopt the following metrics to evaluate the empirical performance:

(1) **Marginal Coverage:** For a predictive confidence band $\mathcal{C}(\mathbf{x})$ and test point (\mathbf{x}, y) , the marginal coverage is defined as $\Pr(y \in \mathcal{C}(\mathbf{x}))$. A valid inference procedure should ensure that the empirical coverage satisfies $\Pr(y \in \mathcal{C}(\mathbf{x})) \geq 1 - \alpha$, where α is the target miscoverage rate.

(2) **Band Length:** Given that the empirical coverage exceeds $1 - \alpha$, the efficiency of the method is quantified by the expected length of the confidence band, $\mathbb{E}[\text{length}(\mathcal{C}(\mathbf{x}))]$. Comparisons of band length are only meaningful under the regime $\Pr(y \in \mathcal{C}(\mathbf{x})) \geq 1 - \alpha$, since trivially $\mathcal{C}(\mathbf{x}) = \emptyset$ yields zero length but violates the coverage constraint.

Table 2: Empirical Marginal Coverage (%) of different models for the task of node classification on four datasets with $\alpha = 0.05$. The result takes the average and standard deviation across 20 independent runs.

| Model | Walmart-Trips | House-Bills | Congress | DBLP | Covered? |
|----------------------|-------------------------------|-------------------------------|-------------------------------|-------------------------------|--------------|
| TS | 92.26 \pm 0.31 \times | 91.21 \pm 0.24 \times | 89.04 \pm 0.48 \times | 87.34 \pm 0.25 \times | \times |
| VS | 92.20 \pm 0.18 \times | 91.18 \pm 0.24 \times | 88.99 \pm 0.46 \times | 87.33 \pm 0.29 \times | \times |
| ETS | 92.20 \pm 0.26 \times | 92.93 \pm 1.77 \times | 89.23 \pm 0.44 \times | 88.29 \pm 0.65 \times | \times |
| CP-APS | 95.17 \pm 0.00 \checkmark | 99.83 \pm 0.09 \checkmark | 99.61 \pm 0.02 \checkmark | 95.04 \pm 0.04 \checkmark | \checkmark |
| CP-RAPS | 95.11 \pm 0.06 \checkmark | 95.20 \pm 0.04 \checkmark | 95.17 \pm 0.04 \checkmark | 95.13 \pm 0.03 \checkmark | \checkmark |
| CF-HGNN-APS | 95.05 \pm 0.01 \checkmark | 99.97 \pm 0.00 \checkmark | 99.94 \pm 0.01 \checkmark | 97.31 \pm 2.58 \checkmark | \checkmark |
| CF-HGNN-RAPS | 95.01 \pm 0.01 \checkmark | 95.18 \pm 0.10 \checkmark | 95.14 \pm 0.07 \checkmark | 95.07 \pm 0.01 \checkmark | \checkmark |
| CCF-HGNN-APS (Ours) | 95.06 \pm 0.32 \checkmark | 99.68 \pm 0.00 \checkmark | 99.79 \pm 0.12 \checkmark | 99.49 \pm 0.39 \checkmark | \checkmark |
| CCF-HGNN-RAPS (Ours) | 95.06 \pm 0.00 \checkmark | 95.33 \pm 0.03 \checkmark | 95.34 \pm 0.34 \checkmark | 95.06 \pm 0.04 \checkmark | \checkmark |

4.2 RESULTS

We will now provide empirical performances of all the baselines and our proposed framework to quantify uncertainty for classification tasks on the four datasets. The important conclusions derived from the experiments are listed below.

All Conformal Frameworks Achieve the Desired Empirical Marginal Coverage while Traditional UQ Methods do not: We report the marginal coverage of various UQ methods with target coverage at 95% in Table 2. There are two primary takeaways. Firstly, none of the traditional UQ methods (VS, TS, and ETS) achieves the target coverage for all datasets, while the conformal prediction methods (CP, CF-HGNN, and CCF-HGNN) do, highlighting the need for models with statistical guarantees when deployed in high-stakes environments. Secondly, these empirical results of all the conformal methods align with the theoretical coverage guarantee given in Lemma 1. Henceforth, we will only report the performance of models that obtain the desired coverage levels.

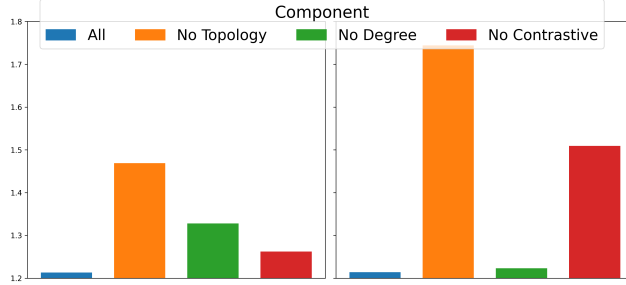
Our Proposed Framework (CCF-HGNN) achieves the shortest Band Length in Most Datasets: We report the empirical band length for 4 datasets in Table 3. The key observations are as follows. First, compared to standard conformal baselines (CP-APS, CP-RAPS). Our proposed approach CCF-HGNN-RAPS produces tighter bands across all but one dataset, while maintaining an impressive overall rank of 1.5 (the closest baselines get to 2.5). Second, while CF-HGNN offers improvements over GNN-based conformal methods, it is consistently outperformed by the proposed CCF-HGNN on hypergraph datasets. These results validate that incorporating contrastive learning with conformal prediction is crucial for boosting efficiency without compromising validity.

378
 379 Table 3: Empirical Predictive Band Length of Different Models (that have the desired coverage level)
 380 on Four Datasets with $\alpha = 0.05$. The result takes the average and standard deviation across 20
 381 independent runs. Lower is better.

| Model | Walmart-Trips | House-Bills | Congress | DBLP | Rank |
|----------------------|-------------------------------------|-------------------------------------|-------------------------------------|-------------------|------------|
| CP-APS | 9.198 \pm 0.048 | 1.958 \pm 0.005 | 1.961 \pm 0.007 | 3.479 \pm 0.127 | 5.0 |
| CP-RAPS | 9.053 \pm 0.008 | 1.261 \pm 0.054 | 1.317 \pm 0.007 | 1.509 \pm 0.038 | 2.5 |
| CF-HGNN-APS | 8.541 \pm 0.023 | 1.993 \pm 0.013 | 1.989 \pm 0.008 | 4.346 \pm 0.387 | 5.0 |
| CF-HGNN-RAPS | 8.595 \pm 0.400 | 1.646 \pm 0.191 | 1.619 \pm 0.129 | 1.977 \pm 0.184 | 3.25 |
| CCF-HGNN-APS (Ours) | 8.481 \pm 0.007 | 1.953 \pm 0.010 | 1.949 \pm 0.008 | 4.354 \pm 1.014 | 3.75 |
| CCF-HGNN-RAPS (Ours) | 8.528 \pm 0.162 | 1.189 \pm 0.027 | 1.213 \pm 0.043 | 1.541 \pm 0.060 | 1.5 |

382 As observed in Table 2, APS-based conformal methods often produce empirical coverage well
 383 above the target level (close to 99%). This behavior arises because APS adaptively accumulates
 384 class probabilities until the calibration cutoff is exceeded, which in practice tends to overshoot
 385 the nominal threshold. While this conservativeness ensures validity, it also leads to overly large
 386 prediction sets. Consequently, APS methods trade efficiency for coverage, resulting in inflated
 387 band lengths (Table 3). By contrast, RAPS introduces an explicit penalty on the set size, thereby
 388 reducing redundancy in the prediction sets while still maintaining the desired coverage guarantees.
 389 However, Walmart-Trips is an exception as the difference between APS and RAPS is less
 390 pronounced, with APS achieving competitive band lengths relative to RAPS. This can be attributed
 391 to the nature of Walmart-Trips, which has a relatively large number of classes (11) but moderate
 392 class imbalance. In such settings, APS’s conservative accumulation of probabilities does not inflate
 393 the prediction sets as severely as in smaller-class datasets, since the distribution of probabilities
 394 is already more spread out across labels. As a result, while RAPS still improves efficiency, the
 395 margin of improvement over APS is narrower on Walmart-Trips compared to the other datasets.
 396

401
 402 **Ablation Study:** We analyze
 403 the effect of removing three key
 404 components—the *topological-aware*
 405 *conformal loss*, *auxillary degree*
 406 *prediction loss*, and *contrastive loss*—
 407 on the **Congress** and **House-Bills**
 408 datasets on at a time. Figure 2 reports
 409 coverage and band length under
 410 RAPS with $\alpha = 0.05$. Our key
 411 observations are: (1) *Topology-aware*
 412 *conformal prediction loss is crucial*:
 413 removing it inflates RAPS length
 414 substantially (e.g., $1.213 \rightarrow 1.469$
 415 on Congress, $1.214 \rightarrow 1.744$ on
 416 House-Bills), showing that structural
 417 information yields tighter sets. (2) *Minimizing the auxillary loss helps*: excluding degree modestly
 418 increases lengths (e.g., $1.213 \rightarrow 1.328$ on Congress). (3) *Contrastive learning improves efficiency*:
 419 dropping it slightly lengthens sets (e.g., $1.213 \rightarrow 1.262$ on Congress). Overall, each component
 420 contributes to efficiency, with topology offering the largest gains. The complete model yields the
 421 tightest bands while maintaining the desired coverage guarantees.



422 Figure 2: Ablation Study: Variation band length (right) for
 423 RAPS on CCF-HGNN on Congress (left) and House-Bills
 424 (right) dataset due to removal of individual components for
 425 $\alpha = 0.05$. Smaller is better.

426 Table 4: Effect of different contrastive strategies (mean \pm std dev across 20 runs.) for $\alpha = 0.05$.

| Dataset | Technique | APS Coverage | APS Length | RAPS Coverage | RAPS Length |
|---------------|----------------|------------------|-------------------|-------------------|-------------------|
| Congress | Hyperedge Drop | 99.83 \pm 0.13 | 1.997 \pm 0.011 | 95.27 \pm 0.19 | 1.309 \pm 0.046 |
| | Edge Drop | 99.79 \pm 0.12 | 1.949 \pm 0.008 | 95.34 \pm 0.034 | 1.213 \pm 0.043 |
| DBLP | Hyperedge Drop | 99.39 \pm 0.10 | 3.688 \pm 0.384 | 95.08 \pm 0.16 | 1.641 \pm 0.132 |
| | Edge Drop | 99.49 \pm 0.39 | 4.354 \pm 1.014 | 95.06 \pm 0.04 | 1.541 \pm 0.060 |
| House-Bills | Hyperedge Drop | 99.68 \pm 0.00 | 1.953 \pm 0.010 | 95.33 \pm 0.03 | 1.189 \pm 0.027 |
| | Edge Drop | 99.64 \pm 0.03 | 1.955 \pm 0.006 | 95.19 \pm 0.00 | 1.214 \pm 0.018 |
| Walmart-Trips | Hyperedge Drop | 95.05 \pm 0.05 | 8.506 \pm 0.136 | 95.05 \pm 0.00 | 8.571 \pm 0.102 |
| | Edge Drop | 95.06 \pm 0.32 | 8.481 \pm 0.007 | 95.06 \pm 0.00 | 8.528 \pm 0.162 |

431 **Sensitivity Study 1: Different Augmentation Strategies** To account for aleatoric uncertainty,
 432 we exploit contrastive augmentations by perturbing the hypergraph structure. We compare two

strategies: (i) *random hyperedge drop*, which removes entire hyperedges, and (ii) *random edge drop*, which removes individual edges in the bipartite node–hyperedge graph. Table 4 summarizes the results. Across datasets, both strategies achieve the target coverage, but their impact on efficiency differs. On **Congress** and **House-Bills**, edge drop consistently yields shorter RAPS sets (e.g., 1.213 vs. 1.309 on Congress), indicating that fine-grained perturbations help the model learn more stable and discriminative representations. In contrast, **DBLP** benefits slightly more from hyperedge drop, where APS sets are tighter (3.688 vs. 4.354), suggesting that larger-scale perturbations are useful in high-homophily graphs with many small hyperedges. For **Walmart-Trips**, the differences between the two strategies are marginal, likely due to its large number of classes and moderate imbalance, where both perturbations introduce comparable variability. Overall, edge drop is generally more effective for heterophilic co-voting datasets, while hyperedge drop can be advantageous for homophilic graphs like DBLP. This demonstrates the importance of tailoring contrastive augmentation strategies to the structural properties of the underlying hypergraph.

Sensitivity Study 2: Dependence on Confidence Level We further study the sensitivity of our method to two key parameters: the miscovariance rate α (i.e., target confidence level) and the calibration set size. Figure 3 shows the results of this experiment for **Congress** and **House-Bills** datasets. Figure 3a and Figure 3b show the change in predic-

tive band length as the confidence level increases from 0.7 to 0.95. Across both datasets, the band length grows monotonically with confidence, as expected. While all methods follow this trend, our method consistently achieves shorter band lengths compared to CP and CF-HGNN, especially at higher confidence levels (e.g., $\alpha = 0.05$). This demonstrates that our contrastive framework yields more informative uncertainty estimates without sacrificing coverage.

Sensitivity Study 3: Size of Calibration Set We also evaluate the effect of calibration set fraction (25%, 50%, 75%). Results in Figure 4a and Figure 4b show that our method remains stable with minimal fluctuation in band length as calibration data decreases. In contrast, CF-HGNN exhibits higher variance and inflated intervals, especially at smaller calibration fractions. This stability highlights the robustness of our approach under limited calibration resources, which is important in real-world healthcare applications where labeled calibration data may be scarce.

Performance in Multi-Class Hypergraph Datasets To additionally observe the performance of the conformal prediction methods for multi-class datasets, we used two datasets, namely **Trivago-Clicks** and **High-School**. The descriptions and summaries of these datasets are provided in Section A.5.

Table 5: APS and RAPS coverage and length across multi-class datasets for $\alpha = 0.05$. Mean \pm standard deviation over 20 runs.

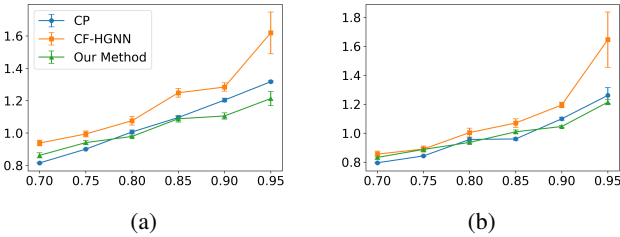


Figure 3: Sensitivity study on varying α for Congress (3a) and House-Bills (3b).

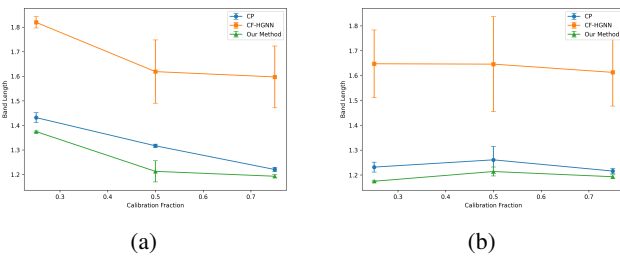


Figure 4: Sensitivity Study on varying the calibration set fraction (4a and 4b) for Congress and House-Bills datasets respectively.

486 The results in Table 5 show that all conformal methods maintain the desired marginal coverage
 487 at the target level $\alpha = 0.05$. However, consistent with our observations in the main paper, our
 488 proposed approach achieves notably shorter prediction sets—particularly under RAPS, demonstrating
 489 improved efficiency while preserving valid coverage. On both datasets, our method outperforms CP
 490 and CF-HGNN in terms of band length, with the largest gains observed on **Trivago-Clicks**, where
 491 the high number of classes amplifies the benefits of contrastive regularization and topology-aware
 492 conformal correction. These results further confirm that jointly modeling aleatoric and epistemic
 493 uncertainties yields tighter and more informative prediction sets in multi-class hypergraph settings.

495 5 RELATED WORKS

497 In this section, we briefly discuss some important works that have not been discussed before. For a
 498 more comprehensive survey, refer to Appendix A.7.

499 (1) Uncertainty Quantification (UQ) on Networks: Traditional UQ methods on graph have gained
 500 more popularity over time Zhao et al. (2020); Stadler et al. (2021); Bertozzi et al. (2018); Han et al.
 501 (2025); Srinivasan et al. (2018) that has influenced training strategies Kang et al. (2022); Trivedi
 502 et al. (2024a) and other applications Huang & Chung (2020); Yu et al. (2024). While some methods
 503 have been proposed for hypergraphs Yao et al. (2025); Harit & Sun (2025), they are focused towards
 504 applications and not generalizable.

505 (2) Conformal Prediction: Due to the statistical guarantee and distribution-free assumptions, con-
 506 formal prediction has become very popular in recent times. Some directions include conditional
 507 conformal prediction Ding et al. (2023); Gibbs et al. (2025); Luo & Zhou (2025), reformulation of
 508 conformal prediction to other domains Correia et al. (2024); Cherian et al. (2024) and conformal
 509 prediction under distribution shift Barber et al. (2023); Clarkson (2023); Thopalli et al. (2025).

511 6 CONCLUSION

513 In this work, we extend the notion of UQ on hypergraphs by jointly accounting for both aleatoric and
 514 epistemic sources of uncertainty and proposing a hypergraph-based conformal prediction framework
 515 that leads to improved band lengths. While this is a promising direction, potential directions of
 516 future work include the evaluation of the performance of other HGNN models like Allset Chien
 517 et al. (2021), ED-HNN Wang et al. (2023a), and accounting for other sources of aleatoric uncertainty.
 518 On the side of conformal prediction, possible future directions include evaluation in the inductive
 519 setting Zargarbashi & Bojchevski (2023); Clarkson (2023) where the assumption of exchangeability
 520 is not maintained.

540 REFERENCES
541

542 Sameer Agarwal, Kristin Branson, and Serge Belongie. Higher order learning with graphs. In
543 *Proceedings of the 23rd international conference on Machine learning*, pp. 17–24, 2006.

544 Ilya Amburg, Nate Veldt, and Austin Benson. Clustering in graphs and hypergraphs with categorical
545 edge labels. In *Proceedings of the web conference 2020*, pp. 706–717, 2020.

546 Anastasios Angelopoulos, Stephen Bates, Jitendra Malik, and Michael I Jordan. Uncertainty sets for
547 image classifiers using conformal prediction. *arXiv preprint arXiv:2009.14193*, 2020.

548 Anastasios N Angelopoulos and Stephen Bates. A gentle introduction to conformal prediction and
549 distribution-free uncertainty quantification. *arXiv preprint arXiv:2107.07511*, 2021.

550 Song Bai, Feihu Zhang, and Philip HS Torr. Hypergraph convolution and hypergraph attention.
551 *Pattern Recognition*, 110:107637, 2021.

552 Rina Foygel Barber, Emmanuel J Candes, Aaditya Ramdas, and Ryan J Tibshirani. Conformal
553 prediction beyond exchangeability. *The Annals of Statistics*, 51(2):816–845, 2023.

554 Stephen Bates, Anastasios Angelopoulos, Lihua Lei, Jitendra Malik, and Michael Jordan. Distribution-
555 free, risk-controlling prediction sets. *Journal of the ACM (JACM)*, 68(6):1–34, 2021.

556 Peter W Battaglia, Jessica B Hamrick, Victor Bapst, Alvaro Sanchez-Gonzalez, Vinicius Zambaldi,
557 Mateusz Malinowski, Andrea Tacchetti, David Raposo, Adam Santoro, Ryan Faulkner, et al.
558 Relational inductive biases, deep learning, and graph networks. *arXiv preprint arXiv:1806.01261*,
559 2018.

560 Andrea L Bertozzi, Xiyang Luo, Andrew M Stuart, and Konstantinos C Zygalakis. Uncertainty
561 quantification in graph-based classification of high dimensional data. *SIAM/ASA Journal on*
562 *Uncertainty Quantification*, 6(2):568–595, 2018.

563 Ting Chen, Simon Kornblith, Mohammad Norouzi, and Geoffrey Hinton. A simple framework for
564 contrastive learning of visual representations. In *International conference on machine learning*, pp.
565 1597–1607. PMLR, 2020.

566 John Cherian, Isaac Gibbs, and Emmanuel Candes. Large language model validity via enhanced
567 conformal prediction methods. *Advances in Neural Information Processing Systems*, 37:114812–
568 114842, 2024.

569 Eli Chien, Chao Pan, Jianhao Peng, and Olgica Milenkovic. You are allset: A multiset function
570 framework for hypergraph neural networks. *arXiv preprint arXiv:2106.13264*, 2021.

571 Philip S Chodrow, Nate Veldt, and Austin R Benson. Generative hypergraph clustering: From
572 blockmodels to modularity. *Science Advances*, 7(28):eab1303, 2021.

573 Akash Choudhuri, Hieu Vu, Kishlay Jha, and Bijaya Adhikari. Domain knowledge augmented
574 contrastive learning on dynamic hypergraphs for improved health risk prediction. In *Proceedings*
575 *of the 2025 SIAM International Conference on Data Mining (SDM)*, pp. 476–486. SIAM, 2025a.

576 Akash Choudhuri, Yongjian Zhong, and Bijaya Adhikari. Implicit hypergraph neural network. *arXiv*
577 *preprint arXiv:2508.14101*, 2025b.

578 Akash Choudhuri, Yongjian Zhong, Mehrdad Moharrami, Christine Klymko, Mark Heimann, Jayaraman
579 J Thiagarajan, and Bijaya Adhikari. Conformal edge-weight prediction in latent space. In
580 *Proceedings of the 2025 SIAM International Conference on Data Mining (SDM)*, pp. 161–170.
581 SIAM, 2025c.

582 Jase Clarkson. Distribution free prediction sets for node classification. In *International conference*
583 *on machine learning*, pp. 6268–6278. PMLR, 2023.

584 Alvaro Correia, Fabio Valerio Massoli, Christos Louizos, and Arash Behboodi. An information
585 theoretic perspective on conformal prediction. *Advances in Neural Information Processing Systems*,
586 37:101000–101041, 2024.

594 Ed Davis, Ian Gallagher, Daniel John Lawson, and Patrick Rubin-Delanchy. Valid conformal
 595 prediction for dynamic gnns. *arXiv preprint arXiv:2405.19230*, 2024.
 596

597 Tiffany Ding, Anastasios Angelopoulos, Stephen Bates, Michael Jordan, and Ryan J Tibshirani. Class-
 598 conditional conformal prediction with many classes. *Advances in neural information processing*
 599 *systems*, 36:64555–64576, 2023.

600 Sofiane Ennadir, Amr Alkhatib, Henrik Bostrom, and Michalis Vazirgiannis. Conformalized adver-
 601 sarial attack detection for graph neural networks. In *Conformal and Probabilistic Prediction with*
 602 *Applications*, pp. 311–323. PMLR, 2023.

603 Yifan Feng, Haoxuan You, Zizhao Zhang, Rongrong Ji, and Yue Gao. Hypergraph neural networks.
 604 In *Proceedings of the AAAI conference on artificial intelligence*, volume 33, pp. 3558–3565, 2019.
 605

606 James H Fowler. Legislative cosponsorship networks in the us house and senate. *Social networks*, 28
 607 (4):454–465, 2006.

608 Yarin Gal and Zoubin Ghahramani. Dropout as a bayesian approximation: Representing model
 609 uncertainty in deep learning. In *international conference on machine learning*, pp. 1050–1059.
 610 PMLR, 2016.

611 Isaac Gibbs and Emmanuel Candes. Adaptive conformal inference under distribution shift. *Advances*
 612 *in Neural Information Processing Systems*, 34:1660–1672, 2021.

613 Isaac Gibbs, John J Cherian, and Emmanuel J Candès. Conformal prediction with conditional
 614 guarantees. *Journal of the Royal Statistical Society Series B: Statistical Methodology*, pp. qkaf008,
 615 2025.

616 Chuan Guo, Geoff Pleiss, Yu Sun, and Kilian Q Weinberger. On calibration of modern neural
 617 networks. In *International conference on machine learning*, pp. 1321–1330. PMLR, 2017.

618 Will Hamilton, Zhitao Ying, and Jure Leskovec. Inductive representation learning on large graphs.
 619 *Advances in neural information processing systems*, 30, 2017.

620 Shen Han, Zhiyao Zhou, Jiawei Chen, Zhezheng Hao, Sheng Zhou, Gang Wang, Yan Feng, Chun
 621 Chen, and Can Wang. Uncertainty-aware graph structure learning. In *Proceedings of the ACM on*
 622 *Web Conference 2025*, pp. 4863–4874, 2025.

623 Anoushka Harit and Zhongtian Sun. Causal spherical hypergraph networks for modelling social
 624 uncertainty. *arXiv preprint arXiv:2506.17840*, 2025.

625 Hans Hao-Hsun Hsu, Yuesong Shen, Christian Tomani, and Daniel Cremers. What makes graph
 626 neural networks miscalibrated? *Advances in Neural Information Processing Systems*, 35:13775–
 627 13786, 2022.

628 Jing Huang and Jie Yang. Unignn: a unified framework for graph and hypergraph neural networks.
 629 *arXiv preprint arXiv:2105.00956*, 2021.

630 Kexin Huang, Ying Jin, Emmanuel Candes, and Jure Leskovec. Uncertainty quantification over graph
 631 with conformalized graph neural networks. *Advances in Neural Information Processing Systems*,
 632 36, 2024.

633 Yongxiang Huang and Albert CS Chung. Edge-variational graph convolutional networks for
 634 uncertainty-aware disease prediction. In *International Conference on Medical Image Computing*
 635 and *Computer-Assisted Intervention*, pp. 562–572. Springer, 2020.

636 Rafael Izbicki, Gilson T Shimizu, and Rafael B Stern. Flexible distribution-free conditional predictive
 637 bands using density estimators. *arXiv preprint arXiv:1910.05575*, 2019.

638 Eric Jang, Shixiang Gu, and Ben Poole. Categorical reparameterization with gumbel-softmax. *arXiv*
 639 *preprint arXiv:1611.01144*, 2016.

640 Jian Kang, Qinghai Zhou, and Hanghang Tong. Jurygcn: quantifying jackknife uncertainty on graph
 641 convolutional networks. In *Proceedings of the 28th ACM SIGKDD Conference on Knowledge*
 642 *Discovery and Data Mining*, pp. 742–752, 2022.

648 Thomas N Kipf and Max Welling. Semi-supervised classification with graph convolutional networks.
 649 *arXiv preprint arXiv:1609.02907*, 2016.
 650

651 Bhawesh Kumar, Charlie Lu, Gauri Gupta, Anil Palepu, David Bellamy, Ramesh Raskar, and Andrew
 652 Beam. Conformal prediction with large language models for multi-choice question answering.
 653 *arXiv preprint arXiv:2305.18404*, 2023.

654 Balaji Lakshminarayanan, Alexander Pritzel, and Charles Blundell. Simple and scalable predictive
 655 uncertainty estimation using deep ensembles. *Advances in neural information processing systems*,
 656 30, 2017.

657

658 Dong Li, Zhiming Xu, Sheng Li, and Xin Sun. Link prediction in social networks based on hypergraph.
 659 In *Proceedings of the 22nd international conference on world wide web*, pp. 41–42, 2013.

660 Xiaoyu Li, Guangyu Tang, and Jiaoqiao Jiang. Implicit hypergraph neural networks: A sta-
 661 ble framework for higher-order relational learning with provable guarantees. *arXiv preprint*
 662 *arXiv:2508.09427*, 2025.

663

664 Zhen Lin, Shubhendu Trivedi, and Jimeng Sun. Conformal prediction with temporal quantile
 665 adjustments. *Advances in Neural Information Processing Systems*, 35:31017–31030, 2022.

666

667 Zong-Zhi Lin, Thomas D Pike, Mark M Bailey, and Nathaniel D Bastian. A hypergraph-based
 668 machine learning ensemble network intrusion detection system. *IEEE transactions on systems,*
 669 *man, and cybernetics: systems*, 2024.

670

671 Rui Luo and Nicolo Colombo. Conformal load prediction with transductive graph autoencoders.
 672 *arXiv preprint arXiv:2406.08281*, 2024.

673

674 Rui Luo and Zhixin Zhou. Conditional conformal risk adaptation. *arXiv preprint arXiv:2504.07611*,
 675 2025.

676

677 Rossana Mastrandrea, Julie Fournet, and Alain Barrat. Contact patterns in a high school: a comparison
 678 between data collected using wearable sensors, contact diaries and friendship surveys. *PloS one*,
 679 10(9):e0136497, 2015.

680

681 Mark EJ Newman. The structure and function of complex networks. *SIAM review*, 45(2):167–256,
 682 2003.

683

684 Maximilian Nickel, Kevin Murphy, Volker Tresp, and Evgeniy Gabrilovich. A review of relational
 685 machine learning for knowledge graphs. *Proceedings of the IEEE*, 104(1):11–33, 2015.

686

687 Aaron van den Oord, Yazhe Li, and Oriol Vinyals. Representation learning with contrastive predictive
 688 coding. *arXiv preprint arXiv:1807.03748*, 2018.

689

690 Yaniv Ovadia, Emily Fertig, Jie Ren, Zachary Nado, David Sculley, Sebastian Nowozin, Joshua
 691 Dillon, Balaji Lakshminarayanan, and Jasper Snoek. Can you trust your model’s uncertainty?
 692 evaluating predictive uncertainty under dataset shift. *Advances in neural information processing*
 693 *systems*, 32, 2019.

694

695 Yaniv Romano, Evan Patterson, and Emmanuel Candes. Conformalized quantile regression. *Advances*
 696 *in neural information processing systems*, 32, 2019.

697

698 Yaniv Romano, Matteo Sesia, and Emmanuel Candes. Classification with valid and adaptive coverage.
 699 *Advances in Neural Information Processing Systems*, 33:3581–3591, 2020.

700

701 Nabeel Seedat, Jonathan Crabbé, and Mihaela van der Schaar. Data-suite: Data-centric identification
 702 of in-distribution incongruous examples. In *International Conference on Machine Learning*, pp.
 703 19467–19496. PMLR, 2022.

704

705 Gowri Srinivasan, Jeffrey D Hyman, David A Osthuis, Bryan A Moore, Daniel O’Malley, Satish
 706 Karra, Esteban Rougier, Aric A Hagberg, Abigail Hunter, and Hari S Viswanathan. Quantifying
 707 topological uncertainty in fractured systems using graph theory and machine learning. *Scientific*
 708 *reports*, 8(1):11665, 2018.

702 Maximilian Stadler, Bertrand Charpentier, Simon Geisler, Daniel Zügner, and Stephan Günnemann.
 703 Graph posterior network: Bayesian predictive uncertainty for node classification. *Advances in*
 704 *Neural Information Processing Systems*, 34:18033–18048, 2021.

705 Kamilė Stankevičiūtė, Ahmed M Alaa, and Mihaela Van der Schaar. Conformal time-series forecast-
 706 ing. *Advances in neural information processing systems*, 34:6216–6228, 2021.

707 David Stutz, Krishnamurthy Dj Dvijotham, Ali Taylan Cemgil, and Arnaud Doucet. Learning optimal
 708 conformal classifiers. In *International Conference on Learning Representations*, 2022.

709 Dirar Sweidan and Ulf Johansson. Probabilistic prediction in scikit-learn. In *The 18th International*
 710 *Conference on Modeling Decisions for Artificial Intelligence, On-line (from Umeå, Sweden),*
 711 *September 27-30, 2021.*, 2021.

712 Jiaye Teng, Chuan Wen, Dinghuai Zhang, Yoshua Bengio, Yang Gao, and Yang Yuan. Predictive
 713 inference with feature conformal prediction. In *The Eleventh International Conference on Learning*
 714 *Representations*, 2022.

715 Kowshik Thopalli, Vivek Narayanaswamy, and Jayaraman J Thiagarajan. The surprising utility of
 716 group partitioning in improving conformal prediction of visual classifiers under distributional
 717 shifts. In *Proceedings of the Computer Vision and Pattern Recognition Conference*, pp. 1742–1751,
 718 2025.

719 Ze Tian, TaeHyun Hwang, and Rui Kuang. A hypergraph-based learning algorithm for classifying
 720 gene expression and arraycgh data with prior knowledge. *Bioinformatics*, 25(21):2831–2838,
 721 2009.

722 Ryan J Tibshirani, Rina Foygel Barber, Emmanuel Candes, and Aaditya Ramdas. Conformal
 723 prediction under covariate shift. *Advances in neural information processing systems*, 32, 2019.

724 Puja Trivedi, Mark Heimann, Rushil Anirudh, Danai Koutra, and Jayaraman J Thiagarajan. A
 725 stochastic centering framework for improving calibration in graph neural networks. In *The Twelfth*
 726 *International Conference on Learning Representations*, 2023.

727 Puja Trivedi, Mark Heimann, Rushil Anirudh, Danai Koutra, and Jayaraman J Thiagarajan. Accurate
 728 and scalable estimation of epistemic uncertainty for graph neural networks. *arXiv preprint*
 729 *arXiv:2401.03350*, 2024a.

730 Puja Trivedi, Danai Koutra, and Jayaraman J Thiagarajan. On estimating link prediction uncertainty
 731 using stochastic centering. In *ICASSP 2024-2024 IEEE International Conference on Acoustics,*
 732 *Speech and Signal Processing (ICASSP)*, pp. 6810–6814. IEEE, 2024b.

733 Aad W Van der Vaart. *Asymptotic statistics*, volume 3. Cambridge university press, 2000.

734 Ashish Vaswani, Noam Shazeer, Niki Parmar, Jakob Uszkoreit, Llion Jones, Aidan N Gomez, Łukasz
 735 Kaiser, and Illia Polosukhin. Attention is all you need. *Advances in neural information processing*
 736 *systems*, 30, 2017.

737 Petar Veličković, Guillem Cucurull, Arantxa Casanova, Adriana Romero, Pietro Lio, Yoshua Bengio,
 738 et al. Graph attention networks. *stat*, 1050(20):10–48550, 2017.

739 Vladimir Vovk, Alexander Gammerman, and Glenn Shafer. *Algorithmic learning in a random world*,
 740 volume 29. Springer, 2005.

741 Peihao Wang, Shenghao Yang, Yunyu Liu, Zhangyang Wang, and Pan Li. Equivariant hypergraph
 742 diffusion neural operators. In *The Eleventh International Conference on Learning Representations*,
 743 2023a. URL <https://openreview.net/forum?id=RiTjKoscnNd>.

744 Tu Wang, Jian Kang, Yujun Yan, Adithya Kulkarni, and Dawei Zhou. Non-exchangeable confor-
 745 mal prediction for temporal graph neural networks. In *Proceedings of the 31st ACM SIGKDD*
 746 *Conference on Knowledge Discovery and Data Mining V*. 2, pp. 3031–3042, 2025.

747 Xiao Wang, Hongrui Liu, Chuan Shi, and Cheng Yang. Be confident! towards trustworthy graph
 748 neural networks via confidence calibration. *Advances in Neural Information Processing Systems*,
 749 34:23768–23779, 2021.

756 Yuxin Wang, Quan Gan, Xipeng Qiu, Xuanjing Huang, and David Wipf. From hypergraph energy
 757 functions to hypergraph neural networks. In *International Conference on Machine Learning*, pp.
 758 35605–35623. PMLR, 2023b.

759
 760 Tianxin Wei, Yuning You, Tianlong Chen, Yang Shen, Jingrui He, and Zhangyang Wang. Aug-
 761 mentations in hypergraph contrastive learning: Fabricated and generative. *Advances in neural*
 762 *information processing systems*, 35:1909–1922, 2022.

763 Hugo Werner, Lars Carlsson, Ernst Ahlberg, and Henrik Boström. Evaluation of updating strategies
 764 for conformal predictive systems in the presence of extreme events. In *Conformal and Probabilistic*
 765 *Prediction and Applications*, pp. 229–242. PMLR, 2021.

766 Ran Xu, Yue Yu, Chao Zhang, Mohammed K Ali, Joyce C Ho, and Carl Yang. Counterfactual
 767 and factual reasoning over hypergraphs for interpretable clinical predictions on ehr. In *Machine*
 768 *Learning for Health*, pp. 259–278. PMLR, 2022.

769 Ran Xu, Mohammed K Ali, Joyce C Ho, and Carl Yang. Hypergraph transformers for ehr-based
 770 clinical predictions. *AMIA Summits on Translational Science Proceedings*, 2023:582, 2023.

771
 772 Naganand Yadati, Madhav Nimishakavi, Prateek Yadav, Vikram Nitin, Anand Louis, and Partha
 773 Talukdar. Hypergcn: A new method for training graph convolutional networks on hypergraphs.
 774 *Advances in neural information processing systems*, 32, 2019.

775
 776 Hong-Yu Yao, Chun-Yang Zhang, Qian-Xi Tang, and CL Philip Chen. Investigating all uncertainties
 777 in hypergraph representation learning and inference. *IEEE Transactions on Fuzzy Systems*, 33(8):
 778 2867–2881, 2025.

779 Rex Ying, Ruining He, Kaifeng Chen, Pong Eksombatchai, William L Hamilton, and Jure Leskovec.
 780 Graph convolutional neural networks for web-scale recommender systems. In *Proceedings of the*
 781 *24th ACM SIGKDD international conference on knowledge discovery & data mining*, pp. 974–983,
 782 2018.

783 Linlin Yu, Yifei Lou, and Feng Chen. Uncertainty-aware graph-based hyperspectral image classifica-
 784 tion. Proceeding of the International Conference on Learning Representations (ICLR), 2024.

785
 786 Margaux Zaffran, Olivier Féron, Yannig Goude, Julie Josse, and Aymeric Dieuleveut. Adaptive
 787 conformal predictions for time series. In *International Conference on Machine Learning*, pp.
 788 25834–25866. PMLR, 2022.

789 Soroush H Zargarbashi and Aleksandar Bojchevski. Conformal inductive graph neural networks. In
 790 *The Twelfth International Conference on Learning Representations*, 2023.

791
 792 Soroush H Zargarbashi, Simone Antonelli, and Aleksandar Bojchevski. Conformal prediction sets
 793 for graph neural networks. In *International Conference on Machine Learning*, pp. 12292–12318.
 794 PMLR, 2023.

795 Huan Zhang, Tsui-Wei Weng, Pin-Yu Chen, Cho-Jui Hsieh, and Luca Daniel. Efficient neural
 796 network robustness certification with general activation functions. *Advances in neural information*
 797 *processing systems*, 31, 2018a.

798
 799 Jize Zhang, Bhavya Kailkhura, and T Yong-Jin Han. Mix-n-match: Ensemble and compositional
 800 methods for uncertainty calibration in deep learning. In *International conference on machine*
 801 *learning*, pp. 11117–11128. PMLR, 2020.

802 Liyan Zhang, Jingfeng Guo, Jiazheng Wang, Jing Wang, Shanshan Li, and Chunying Zhang. Hyper-
 803 graph and uncertain hypergraph representation learning theory and methods. *Mathematics*, 10(11):
 804 1921, 2022.

805 Zizhao Zhang, Haojie Lin, Yue Gao, and KLISS BNRIst. Dynamic hypergraph structure learning. In
 806 *IJCAI*, pp. 3162–3169, 2018b.

807
 808 Tianyi Zhao, Jian Kang, and Lu Cheng. Conformalized link prediction on graph neural networks. In
 809 *Proceedings of the 30th ACM SIGKDD Conference on Knowledge Discovery and Data Mining*, pp.
 4490–4499, 2024.

810 Xujiang Zhao, Feng Chen, Shu Hu, and Jin-Hee Cho. Uncertainty aware semi-supervised learning on
811 graph data. *Advances in neural information processing systems*, 33:12827–12836, 2020.
812
813
814
815
816
817
818
819
820
821
822
823
824
825
826
827
828
829
830
831
832
833
834
835
836
837
838
839
840
841
842
843
844
845
846
847
848
849
850
851
852
853
854
855
856
857
858
859
860
861
862
863

864 7 LLM USAGE AND ETHICS STATEMENT
865

866 This paper presents work whose goal is to advance the field of Representation Learning. There
867 are many potential societal consequences of our work, none of which we feel must be specifically
868 highlighted here. LLMs were used to correct grammatical errors that originated during the writing of
869 the manuscript. LLMs were not used to create any ideas. Our source code and experimental setup
870 are provided through the anonymised link in the manuscript. All the datasets used in this work are
871 publicly available, and there are no competing interests.

872
873 A APPENDIX
874875 A.1 HYPERGRAPH NEURAL NETWORKS
876

877 The early structure of HGNNs mimicked the convolution step of GNNs. In particular, Feng et al. Feng
878 et al. (2019) proposed the first spectral hypergraph convolution, formulated as

$$879 \mathbf{X}' = \sigma \left(\mathbf{D}_v^{-\frac{1}{2}} \mathbf{H} \mathbf{W}_e \mathbf{D}_e^{-1} \mathbf{H}^\top \mathbf{D}_v^{-\frac{1}{2}} \mathbf{X} \mathbf{W} \right), \quad (5)$$

880 where \mathbf{H} is the incidence matrix, \mathbf{D}_v and \mathbf{D}_e are vertex and hyperedge degree matrices, \mathbf{W}_e is a
881 diagonal hyperedge weight matrix, and \mathbf{W} is a trainable weight matrix.

882 Later, Bai et al. (2021) introduced a simplified hypergraph convolution operation, expressed as

$$883 \mathbf{X}' = \sigma \left(\mathbf{D}_v^{-1} \mathbf{H} \mathbf{D}_e^{-1} \mathbf{H}^\top \mathbf{X} \mathbf{W} \right), \quad (6)$$

884 which removes the symmetric normalization and leads to a message-passing view of hypergraph
885 learning. This formulation laid the foundation for subsequent works such as UniGNN Huang & Yang
886 (2021). In all our experiments, we have used the formulation by Bai et al. (2021).

887 A.2 PROOF OF LEMMA 2
888

889 *Proof.* From Proposition E.2 in Oord et al. (2018), we know

$$890 I(Y; \mathbf{Z}) \geq \log(N) - \mathcal{L}_{\mathbf{Z}}^{\text{InfoNCE}},$$

891 where N is the number of samples and $\mathcal{L}_{\mathbf{Z}}^{\text{InfoNCE}}$ the InfoNCE loss.

892 For our method, $\mathcal{L}_{\mathbf{Z}_1}^{\text{InfoNCE}}$ is explicitly minimized, compared to CF-HGNN, which consequently
893 means that $\log(N) - \mathcal{L}_{\mathbf{Z}_1}^{\text{InfoNCE}} \geq \log(N) - \mathcal{L}_{\mathbf{Z}_0}^{\text{InfoNCE}}$.

894 This implies the proof statement:

$$895 I(Y; \mathbf{Z}_1) \geq I(Y; \mathbf{Z}_0) + \Delta$$

□

900 A.3 PROOF OF THEOREM 1
901

902 **Lemma 3.** Correia et al. (2024) For any conformal prediction scheme with the coverage guarantee
903 of $1 - \alpha$, and any distribution $q(\cdot)$, we have:

$$904 \mathbb{E}([\log |\mathcal{C}(x)|]^+) \geq \\ 905 (1 - \alpha) \frac{H(Y|X) - h_b(a) - a \log M - \alpha \mathbb{E}_{P_{Y,X,D_{cal}|E=0}} \left[-\log \hat{Q}_{Y|X}^0 + \log \mathbb{E}_{u(y_{\mathcal{C}(x)})} [q(y|x)] \right]}{1 - \alpha + \frac{1}{n+1}} \\ 906 - (1 - \alpha) \mathbb{E}_{P_{Y,X,D_{cal}|E=1}} \left[-\log \hat{Q}_{Y|X}^1 + \log \mathbb{E}_{u(y_{\mathcal{C}(x)})} [q(y|x)] \right], \quad (7)$$

907 where $\hat{Q}_{Y|X}^0 = q(y|x) \mathbb{I}[y \notin \mathcal{C}(x)]$ and $\hat{Q}_{Y|X}^1 = q(y|x) \mathbb{I}[y \in \mathcal{C}(x)]$. Here, $|\mathcal{C}(x)|$ denotes the size
908 of the prediction set for input x , $H(Y|X)$ the conditional entropy of Y given X , $h_b(\cdot)$ the binary
909 entropy function, a the error probability, and $M = |\mathcal{Y}|$ the number of classes.

918 Algorithm 1 Contrastive Hypergraph Conformal Prediction (CCF-HGNN)

919 Input: Hypergraph $H = \{\mathcal{V}, \mathcal{E}\}$, feature matrix \mathbf{X} , label set \mathcal{Y} , Incidence Matrix H
920 HGNN train Model $\hat{\mu}(\cdot)$, calibration model $\tilde{\mu}(\cdot)$ with weights ϑ , non-conformity score function
921 $V(\cdot, \cdot)$, Calibration dataset \mathcal{D}_{cal} partitioned into $\mathcal{D}_{\text{corr-cal}} = \{(\mathbf{x}_i, y_i)\}_{i=1}^{n_{\text{corr-cal}}}$,
922 and $\mathcal{D}_{\text{cal-test}} = \{(\mathbf{x}_i, y_i)\}_{i=1}^{n_{\text{cal-test}}}$, significance level α , Hypergraph incidence, node and hyperedge
923 degree matrices $\mathbf{H}, \mathbf{D}_e, \mathbf{D}_v$
924 1: Train HGNN model $\hat{\mu}(H, \mathbf{X})$ on prediction task.
925 2: **while** Not converged **do**
926 3: Obtain augmentations \mathcal{H}_1 and \mathcal{H}_2 of H .
927 4: Compute the hyperedge Laplacians \mathbf{L}_1 and \mathbf{L}_2 , corresponding attention weights \mathbf{a}^1 and \mathbf{a}^2 .
928 5: Select the k important hyperedges using the Gumbel-Softmax trick.
929 6: Compute the overall degree loss $\mathcal{L}_{\text{deg}} = \mathcal{L}_{\text{deg}}^1 + \mathcal{L}_{\text{deg}}^2$.
930 7: Get embeddings $\mathbf{Z}^1 = \tilde{\mu}(\mathcal{H}_1, f(\mathbf{X}))$, $\mathbf{Z}^2 = g(\mathcal{H}_2, f(\mathbf{X}))$.
931 8: Get calibration predictions $\mathbf{Z}_{\text{cal}}^1, \mathbf{Z}_{\text{cal}}^2$ from $\mathbf{Z}^1, \mathbf{Z}^2$.
932 9: Compute $\mathbf{Z}_{\text{cal}} = \frac{\mathbf{Z}_{\text{cal}}^1 + \mathbf{Z}_{\text{cal}}^2}{2}$.
933 10: Get test predictions $\mathbf{Z}_{\text{test}}^1, \mathbf{Z}_{\text{test}}^2$ from $\mathbf{Z}^1, \mathbf{Z}^2$.
934 11: Compute $\mathbf{Z}_{\text{test}} = \frac{\mathbf{Z}_{\text{test}}^1 + \mathbf{Z}_{\text{test}}^2}{2}$.
935 12: Compute $\hat{\alpha} = \frac{1}{n+1} \cdot \alpha$.
936 13: $\hat{\eta} = \text{DiffQuantile}(\{V(\mathbf{Z}_i, y_i) \mid i \in \mathcal{D}_{\text{cal}}\})$.
937 14: $\mathcal{L}_{\text{Ineff}} = \frac{1}{m} \sum_{i \in \mathcal{D}_{\text{cal-test}}} \frac{1}{|\mathcal{Y}|} \sum_{k \in \mathcal{Y}} \sigma\left(\frac{V(\mathbf{z}_i, k) - \hat{\eta}}{\tau_1}\right)$.
938 15: $\mathcal{L}_{\text{Contra}} = \text{INFONCE}(\mathbf{Z}^1, \mathbf{Z}^2, \tau_2)$
939 16: $\mathcal{L}_{\text{Total}} = \gamma \mathcal{L}_{\text{Ineff}} + (1 - \gamma) \mathcal{L}_{\text{Contra}} + \mathcal{L}_{\text{deg}}$.
940 17: $\vartheta = \vartheta - \nabla_{\vartheta} \mathcal{L}_{\text{Total}}$.
941 18: **end while**

942
943
944 Lemma 3 shows that the expected prediction set size is lower bounded by the conditional entropy
945 $H(Y|X)$, penalized by calibration-dependent terms.

946
947 *Proof.* By Lemma 2, $I(Y; Z_1) \geq I(Y; Z_0) + \Delta$. Equivalently, $H(Y|Z_1) \leq H(Y|Z_0) - \Delta$.

948 Lemma 3 lower bounds the expected log set size in terms of $H(Y|X)$. Since Z_1 captures more
949 information about Y than Z_0 , the effective conditional entropy $H(Y|Z_1)$ is smaller. Thus, the bound
950 for $\mathcal{C}_1(X)$ is tighter than for $\mathcal{C}_0(X)$.

951 Formally,

$$\begin{aligned} \mathbb{E}[\log |\mathcal{C}_0(X)|]^+ &\geq f(H(Y|Z_0)), \\ \mathbb{E}[\log |\mathcal{C}_1(X)|]^+ &\geq f(H(Y|Z_1)), \end{aligned}$$

952 where $f(\cdot)$ is the lower-bound functional in Lemma 3. Since $H(Y|Z_1) < H(Y|Z_0)$, the bound for
953 $\mathcal{C}_1(X)$ is strictly smaller, which implies:

$$\mathbb{E}[|\mathcal{C}_1(X)|] \leq \mathbb{E}[|\mathcal{C}_0(X)|].$$

□

A.4 CONVERGENCE OF CCF-HGNN

954
955 **Theorem 2.** If the calibration model $\tilde{\mu}(\cdot)$ produces stable predictions $\hat{p}(y_i|\mathcal{X}_i)$ as the number of
956 calibration samples $n_{\text{cal}} \rightarrow \infty$, the expected prediction set size $\mathbb{E}[|C(\mathbf{x})|]$ for a test point converges
957 in probability to a fixed value:

$$\mathbb{E}[|C(\mathbf{x})|] \rightarrow \sum_{y \in \mathcal{Y}} \mathbb{P}(\hat{p}(y|\mathbf{x}) \geq 1 - q^*), \quad (8)$$

958 where $q^* = F^{-1}(1 - \alpha)$ is the $(1 - \alpha)^{\text{th}}$ -quantile of the true non-conformity score distribution.

972 *Proof.* Let $F_n(v) = \frac{1}{n} \sum_{i=1}^n \mathbf{1}(V_i \leq v)$ be the empirical CDF of the non-conformity scores $V_i = 973 1 - \hat{p}(y_i | \mathcal{X}_i)$.

974 Using Glivenko-Cantelli Theorem Van der Vaart (2000) with Assumption 1, $\sup_v |F_n(v) - F(v)| \rightarrow 975 0$ as $n \rightarrow \infty$. Assuming the calibration model $\tilde{\mu}(\cdot)$ produces stable predictions $\hat{p}(y_i | \mathcal{X}_i)$ as the 976 number of calibration samples $n_{cal} \rightarrow \infty$, and as F is continuous and strictly increasing, F^{-1} is 977 continuous at $1 - \alpha$.

978 For any $\epsilon > 0$, choose $\delta > 0$ such that

$$979 F(q^* - \epsilon) < 1 - \alpha - \delta, \quad F(q^* + \epsilon) > 1 - \alpha + \delta.$$

980 As n_{cal} grows, $\sup_v |F_{n_{cal}}(v) - F(v)| < \delta$, which means

$$981 F_{n_{cal}}(q^* - \epsilon) \geq F(q^* - \epsilon) - \delta < 1 - \alpha,$$

982 and

$$983 F_{n_{cal}}(q^* + \epsilon) \leq F(q^* + \epsilon) + \delta > 1 - \alpha.$$

984 So $q^* - \epsilon < \hat{q} < q^* + \epsilon$, which means

$$985 \mathbb{P}(|\hat{q} - q^*| > \epsilon) \rightarrow 0 \quad \text{as } n_{cal} \rightarrow \infty.$$

986 The prediction set is thus

$$987 C(\mathbf{x}) = \{y \in \mathcal{Y} : \hat{p}(y | \mathbf{x}) \geq 1 - \hat{q}\}.$$

988 So the expected set size is

$$989 \mathbb{E}[|C(\mathbf{x})|] = \mathbb{E} \left[\sum_{y \in \mathcal{Y}} \mathbf{1}(\hat{p}(y | \mathbf{x}) \geq 1 - \hat{q}) \right] = \sum_{y \in \mathcal{Y}} \mathbb{P}(\hat{p}(y | \mathbf{x}) \geq 1 - \hat{q}).$$

990 As $\hat{q} \rightarrow q^*$, and since $g(\cdot)$ is stable,

$$991 \mathbf{1}(\hat{p}(y | \mathbf{x}) \geq 1 - \hat{q}) \rightarrow \mathbf{1}(\hat{p}(y | \mathbf{x}) \geq 1 - q^*).$$

992 So,

$$993 \mathbb{E}[|C(\mathbf{x})|] \rightarrow \sum_{y \in \mathcal{Y}} \mathbb{P}(\hat{p}(y | \mathbf{x}) \geq 1 - q^*).$$

994 This limit is a fixed value determined by the distribution of $\hat{p}(y | \mathbf{x})$ and q^* .

995 Conformal prediction ensures that as long as \hat{q} is calibrated,

$$996 \mathbb{P}(y \in C(\mathbf{x})) \geq 1 - \alpha.$$

1000 \square

1001 A.5 DESCRIPTIONS OF THE DATASETS

1002 Table 6: Statistics of the selected datasets. Here, DBLP is a homophilic dataset while the others are 1003 heterophilic.

| 1004 Property | 1005 DBLP | 1006 Congress | 1007 House-Bills | 1008 Walmart-Trips | 1009 High-School | 1010 Trivago-Clicks |
|----------------------|------------------|----------------------|-------------------------|---------------------------|-------------------------|----------------------------|
| 1011 # nodes | 1012 41,302 | 1013 1,718 | 1014 1,494 | 1015 88,860 | 1016 327 | 1017 170,994 |
| 1018 # hyperedges | 1019 22,363 | 1020 83,105 | 1021 60,987 | 1022 69,906 | 1023 7818 | 1024 232,013 |
| 1025 # classes | 1026 6 | 1027 2 | 1028 2 | 1029 11 | 1030 9 | 1031 80 |
| 1032 avg. $ e $ | 1033 4.452 | 1034 8.656 | 1035 20.500 | 1036 6.589 | 1037 2.300 | 1038 3.116 |

1039 This work uses four hypergraph classification datasets in the main text. They are as follows:

1040 • **Walmart-Trips:** This is a customer recruitment prediction dataset where the hyperedges 1041 are sets of co-purchased products at Walmart. Products (nodes) are assigned to one of ten 1042 broad departments in which the product appears on walmart.com (e.g., "Clothing, Shoes, 1043 and Accessories"), and these serve as node labels (there is also an additional "Other" class).

- **DBLP:** This is a co-authorship hypergraph dataset created by Yadati et al. (2019). It represents collaborations among authors listed in DBLP, the computer science bibliographic database, as of 3 Sept. 2017. Each node represents an author, and each publication is represented by a simplex (a set of nodes, i.e., a hyperedge), timestamped by the year of publication. This is the only homophilic hypergraph dataset
- **Congress:** In this hypergraph dataset, nodes are US Congresspersons and simplices are comprised of the sponsor and co-sponsors of legislative bills put forth in both the House of Representatives and the Senate.
- **House-Bills:** In this hypergraph dataset, nodes are US Congresspersons and hyperedges are the sponsors and co-sponsors of bills put forth in the House of Representatives. Some hyperedges are repeated. Each node is labeled with political party affiliation.

Additionally, this work also used two multi-class hypergraph datasets. They are as follows:

- **High-School** Chodrow et al. (2021); Mastrandrea et al. (2015): This is a static, annotated hypergraph version of the temporal higher-order contact-high-school dataset. Each hyperedge corresponds to a group of people who were all in proximity of one another at a given time, based on data from sensors worn by students. Each node is labeled with the classroom to which the student belongs.
- **Trivago-Clicks** Chodrow et al. (2021): This is a hypergraph, where nodes are accommodations (mostly hotels), and hyperedges are sets of accommodations for which a user performed the "click-out" action during the same browsing session, which means the user was forwarded to a partner site. Although the original dataset has 160 node classes, a lot of them are singular. We selected the nodes belonging to the top 80 labels in our experiments.

A.6 DESCRIPTIONS OF THE BASELINES

The baseline models used in this work can be characterized into the following categories:

- **Traditional UQ Methods:** These methods do not provide any statistical guarantee about marginal coverage. The 3 baseline methods used under this category are as follows:
 1. **Temperature Scaling (TS) Guo et al. (2017):** It is a post-processing calibration method for UQ. It takes the model's logits (pre-softmax outputs) and divides them by a learned scalar parameter called the temperature. Higher temperature values produce softer probability distributions with lower confidence.
 2. **Vector Scaling (VS) Guo et al. (2017):** Vector scaling is a more flexible version of temperature scaling. Instead of using a single global adjustment for all classes, it assigns each class its own adjustment with a small bias. This allows the model to adjust situations where some classes are consistently overconfident or underconfident, thereby improving the calibration of predicted probabilities across all classes.
 3. **Ensemble Temperature Scaling (ETS) Zhang et al. (2020):** Ensemble Temperature Scaling applies temperature scaling to the aggregated outputs of a model ensemble. A single temperature parameter is learned on the ensemble's averaged logits to adjust overall confidence. This method preserves the accuracy advantages of ensembling while improving calibration, resulting in more reliable uncertainty estimates.
- **Conformal Prediction Methods:** These methods have a theoretical guarantee for marginal coverage. We adapted two prior works as baselines:
 1. **Conformal Predictor (CP) Vovk et al. (2005):** For this model, the mean estimator (HGNN) was trained on the classification task on the training data. After that, the non-conformity scores were obtained for the calibration data (node set), a quantile was selected (based on the type of the non-conformity score function), and predictive bands were constructed for test nodes.
 2. **Conformalized Hypergraph Neural Network Huang et al. (2024) (CF-HGNN):** This model integrates conformal prediction with hypergraph neural networks to provide uncertainty estimates with guaranteed marginal coverage. The key idea is to adapt non-conformity scores to hypergraph learning tasks, where nodes, edges, and higher-order relationships need to be considered simultaneously. CF-HGNN first trains a base

1080 HGNN to produce class probability estimates, then applies a conformal calibration
 1081 step using a held-out calibration set. Unlike CP, CF-HGNN explicitly accounts for
 1082 hypergraph structures, leading to tighter predictive sets and better utilization of higher-
 1083 order relational information. As such, it represents the current state-of-the-art approach
 1084 for principled uncertainty quantification in hypergraph datasets, balancing theoretical
 1085 guarantees with strong empirical performance.

1086

1087 A.7 RELATED WORKS

1088

1089 We discuss here related works that are closest to the ideas in CCF-HGNN in this section.

1090 **(1) Uncertainty Quantification in deep learning and GNNs:** Several approaches address model-
 1091 agnostic risk estimation for Graph Neural Networks (GNNs) in both classification and regression
 1092 tasks Zhang et al. (2020); Ovadia et al. (2019); Seedat et al. (2022). Other studies leverage struc-
 1093 tural properties of graphs to explore calibration challenges, particularly the tendency of GNNs to
 1094 be underconfident Wang et al. (2021); Hsu et al. (2022). A foundational perspective is provided
 1095 by Gal & Ghahramani (2016), who interpret dropout training in deep neural networks as approximate
 1096 Bayesian inference in deep Gaussian Processes. Complementary work investigates factors such as
 1097 network depth, width, weight decay, batch normalization, and temperature scaling for improving
 1098 calibration Lakshminarayanan et al. (2017); Guo et al. (2017). More recently, stochastic centering
 1099 has been proposed and applied as an effective calibration technique for GNNs Trivedi et al. (2023;
 1100 2024b).

1101 **(2) Conformal Prediction:** Conformal inference provides distribution-free uncertainty quantification
 1102 with rigorous coverage guarantees, enabling applications across diverse domains such as model
 1103 calibration Sweidan & Johansson (2021), passenger booking systems Werner et al. (2021), computer
 1104 vision Angelopoulos et al. (2020); Bates et al. (2021), and time-series forecasting Gibbs & Candes
 1105 (2021); Lin et al. (2022). Given a user-specified miscoverage rate $\alpha \in (0, 1)$, the framework uses
 1106 a calibration dataset to construct prediction sets or intervals that contain the true outcome with
 1107 probability at least $1 - \alpha$. A variety of nonconformity scores have been proposed to improve
 1108 performance in classification settings Romano et al. (2019; 2020); Izbicki et al. (2019), with recent
 1109 work introducing scores in the latent feature space Teng et al. (2022). While the classical framework
 1110 relies on exchangeability, several extensions relax this assumption to handle label shift, covariate
 1111 shift, or dependent data Gibbs & Candes (2021); Barber et al. (2023); Tibshirani et al. (2019); Lin
 1112 et al. (2022).

1113 **(3) Conformal Prediction for GNNs:** The use of conformal inference for network-structured data has
 1114 recently gained traction. The first application in the inductive setting Clarkson (2023) demonstrated
 1115 that nonconformity scores in this context are not exchangeable. In contrast, subsequent works Huang
 1116 et al. (2024); Zargarbashi et al. (2023); Luo & Colombo (2024) study the transductive setting, where
 1117 nonconformity scores retain exchangeability. These approaches exploit the local neighborhood
 1118 structure of graphs to improve effectiveness while maintaining computational efficiency. More
 1119 recently, Zargarbashi & Bojchevski (2023) introduced the notions of node-exchangeability and edge-
 1120 exchangeability in growing graphs for the inductive setting, and proposed nonconformity scores
 1121 defined on the evolving graph structure at each step. Recent works also include conformalized link
 1122 prediction Zhao et al. (2024), weighted edge prediction Choudhuri et al. (2025c); Luo & Colombo
 1123 (2024), dynamic GNNs Davis et al. (2024); Wang et al. (2025) and adversarial attack detection Ennadir
 et al. (2023).

1124

1125 A.8 ABLATION STUDY: OPTIMIZING OTHER NON-CONFORMITY SCORES

1126

1127 While our main experimental results were based on optimizing APS, we performed an additional
 1128 experiment by using DAPS Zargarbashi et al. (2023) as the non-conformity score function. The
 1129 neighbour diffused scores of DAPS is given by $\hat{\mathbf{H}} = (1 - \lambda)\mathbf{H} + \mathbf{D}^{-1}\mathbf{A}\mathbf{H}$, where \mathbf{D} denotes the
 1130 node degree matrix, \mathbf{A} denotes the node adjacency matrix and \mathbf{H} denotes the node-wise score matrix.
 1131 We experimented on **Walmart-Trips** and **DBLP** datasets for a target coverage of 95%. The results of
 1132 our experiments are presented in Table 7.

1133 We notice that for **Walmart-Trips**, using DAPS does not improve performance for our method
 compared to optimizing the APS score in Table 3. However, the performance of our method improves

1134 Table 7: Average Marginal Coverage and Band Length for all conformal methods using DAPS
 1135 non-conformity score across 20 runs. $\alpha = 0.05$

| 1137 | Dataset | Method | Coverage | Length |
|------|---------------|--------------|------------------|-------------------------------------|
| 1138 | Walmart-Trips | CP-APS | 95.16 ± 0.02 | 8.973 ± 0.003 |
| 1139 | | CP-RAPS | 95.08 ± 0.01 | 8.901 ± 0.053 |
| 1140 | | CF-HGNN-APS | 95.05 ± 0.02 | 8.588 ± 0.003 |
| 1141 | | CF-HGNN-RAPS | 95.01 ± 0.00 | 8.611 ± 0.001 |
| 1142 | | Our-APS | 95.07 ± 0.03 | 8.518 ± 0.001 |
| 1143 | | Our-RAPS | 95.05 ± 0.01 | 8.592 ± 0.003 |
| 1144 | DBLP | CP-APS | 97.05 ± 0.00 | 3.470 ± 0.065 |
| 1145 | | CP-RAPS | 95.07 ± 0.00 | <u>1.600 ± 0.011</u> |
| 1146 | | CF-HGNN-APS | 97.11 ± 0.01 | 3.920 ± 0.011 |
| 1147 | | CF-HGNN-RAPS | 95.08 ± 0.00 | 1.703 ± 0.002 |
| 1148 | | Our-APS | 98.79 ± 0.01 | 3.734 ± 0.067 |
| 1149 | | Our-RAPS | 95.13 ± 0.00 | 1.508 ± 0.067 |

1154 when evaluated on the **DBLP dataset**. This is primarily due to the fact that the non-conformity score
 1155 of DAPS induces homophily and thus does not improve performance in a heterophilous hypergraph
 1156 like **Walmart-Trips**. However, for a homophilous hypergraph like **DBLP**, the performance of all
 1157 methods improves significantly when using an appropriate non-conformity score.

1159 A.9 EFFECT OF MEAN ESTIMATOR ON OUR METHOD

1161 Table 8: Performance of Models using ED-HNN averaged across 20 runs. $\alpha = 0.05$

| 1163 Dataset | Model | APS Coverage | APS Length | RAPS Coverage | RAPS Length |
|------------------|-------|------------------|-----------------|------------------|-----------------|
| 1165 Congress | CP | 99.49 ± 0.00 | 1.95 ± 0.00 | 95.29 ± 0.00 | 1.78 ± 0.12 |
| | Ours | 98.99 ± 0.00 | 1.97 ± 0.02 | 95.28 ± 0.00 | 1.40 ± 0.05 |
| 1167 House-Bills | CP | 99.53 ± 0.00 | 1.95 ± 0.01 | 95.25 ± 0.00 | 1.24 ± 0.07 |
| | Ours | 98.74 ± 0.01 | 1.96 ± 0.03 | 95.19 ± 0.00 | 1.15 ± 0.15 |

1171 The mean estimator used for all experiments in the main text was HCHA Bai et al. (2021). As
 1172 the conformal methods quantify uncertainty estimates on top of the point predictions made by the
 1173 mean estimator, altering the mean estimator will cause fluctuations in performance. To illustrate this
 1174 fact, we used a more recent backbone model, ED-HNN Wang et al. (2023a), that had slightly lower
 1175 validation accuracy than HCHA **Congress** and slightly higher validation accuracy on **House-Bills**
 1176 datasets. The results of our experiment are shown in Table 8.

1177 The experimental results show that using ED-HNN instead of HCHA produces wider uncertainty
 1178 estimates for the **Congress** dataset. On the other hand, for the **House-Bills** dataset, we observe
 1179 slightly shorter predictive bands. This empirically validates the correlation between the predictive
 1180 performance of the mean estimator and the size of the uncertainty bands. The higher the predictive
 1181 accuracy of the mean estimator, the shorter the size of the uncertainty bands, and vice versa.

1183 A.10 SCALABILITY OF CF-HGNN AND OUR METHOD

1185 The limitation of both our method and CF-GNN is that they are more computationally expensive.
 1186 However, this comes at a cost of shorter predictive bands (as the losses encourage shorter band length
 1187 while maintaining desired levels of coverage). On that front, both CF-GNN and our method do not
 take too much time for this optimization in the calibration step. To demonstrate this, we perform an

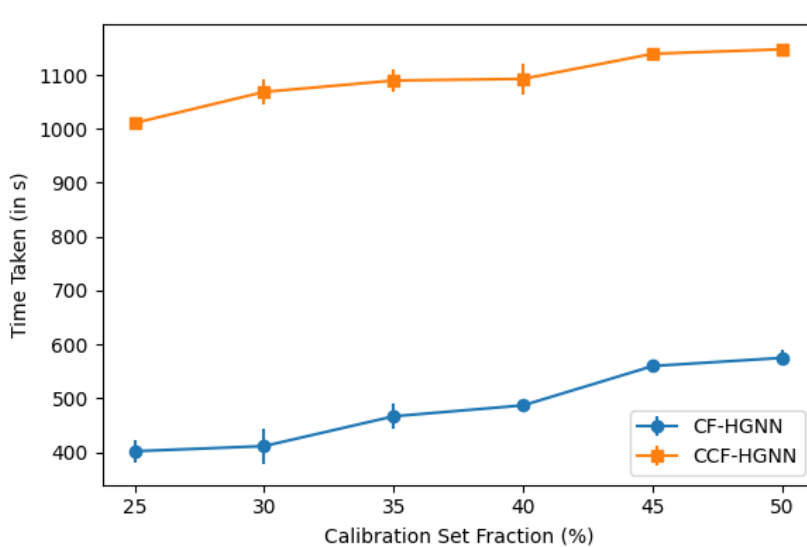


Figure 5: Comparison of total time taken for calibration optimization for both models on different calibration set sizes (averaged across 20 runs).

additional experiment on **Walmart-Trips** dataset by altering the size of the calibration set and noting the total time taken for calibration for 5000 epochs(in s). The results are shown in Figure 5.

While our method takes 2.5x more time than CF-HGNN (due to additions), our method scales by the same rate when increasing the calibration set size. This cost is offset by the improved performance in producing the uncertainty bands.

A.11 EXAMPLES OF VIOLATION OF ASSUMPTION 1 IN THEOREM 2

There are some extreme examples where the contrastive augmentations (structure-altering augmentations) will violate this assumption. They are, as follows:

1. In multi-class node classification with extreme label imbalance, where even small augmentation may disproportionately isolate nodes from minority classes. In such cases, the topology-aware correction mechanism may no longer propagate reliable information through the local neighborhood, causing calibration to break down and resulting in lower empirical marginal coverage on average.
2. Another example occurs in hypergraphs with extremely poor connectivity, such as containing a single bridging hyperedge that connects two or more large, otherwise disconnected hypergraph components. If a contrastive augmentation removes or perturbs this bridging hyperedge, the connectivity between the components is disrupted. As a result, the local neighborhood information used in the topology-aware correction may no longer reflect the true label dependencies across the hypergraph, potentially violating the Bounded Coverage assumption and leading to miscalibrated prediction sets.